Evaluating the Impact of Voltage Imbalance on The Power factor of Three Phase Induction

Abdelhamed Fraj Saleh–Faculty of Engineering, the University of Bani–Waleed, Libya

Abstract

A three-phase squirrel cage motor was modeled to evaluate the impact of voltage imbalance on power factor of such type of motors. The model has been derived using a multi coupled circuits approach. Then a transformation called Hilbert transform was used to convert the input voltage and current into rotating vectors in order to determine the instantaneous power factor. The obtained results show that the power factor of the motor increases as the percentage of voltage imbalance increase.

Index Terms

Voltage imbalance, power factor, induction motor model, Hilbert transform.

Nomenclature

V_m and I_m are the voltage and current RMS values.

ω is the supply frequency.

φ is the instantaneous phase between the input voltage and current.

$\overrightarrow{v_A}$ and $\overrightarrow{i_A}$ are the voltage and current vectors.

j designates the imaginary part.

v_A and i_A are the voltage and current real components.

v_H and i_H are the imaginary voltage and current components.

φ_v is the voltage phase angle.

φ_i is the current phase angle.

V_s, V_r are the stator and rotor voltages.

I_s, I_r are the stator and rotor currents.

R_s, R_r are the stator and rotor resistances.

L_s, L_r are the stator and rotor inductances.

M_{sr} is the mutual inductance between the stator phases and rotor loops.

$V_{s(im)}$ is the stator voltages with voltage imbalance fault.

V_d is the value of the voltage imbalance.

P is the number of pole pairs.

θ is the rotor displacement.

T_{em} is the electromagnetic torque produced by the motor.

T_{el} is the external load applied on the machine shaft.

J is the rotor inertia.

I. introduction

VOLTAGE imbalance occurs when the RMS line voltages on a three phase system are unequal. Generally, in three phase system voltages are rarely balanced, but when this imbalance becomes excessive, it can create problems for three phase motors [1]. There are three possible sources of voltage imbalance for motors; the power supplier, the facility housing the motor, and the motor itself [2]. Regardless of the cause, voltage imbalance generates an excessive heat in the motor windings. This can results in an insulation breakdown. In addition to that, voltage imbalance can create a current imbalance 6 to 10 times the magnitude of voltage imbalance [3]. Consequently, this current imbalance affects the power factor and causes energy losses and hence decreases the efficiency. Although there are several standards recommended for appropriate limits of voltage imbalance such as: ANSI C84.1, PG&E and NEMA, many disputes between customers, motor manufacturers, and the power suppliers have presented [4, 5]. Therefore, careful consideration should be made in each location to the utility's service guidelines to versus the motor

manufacturer's guidelines, to ensure a proper understanding of the two. It is known that a considerable percentage of generated power in the world is consumed by motors [1]. Since voltage imbalance can be very harmful to motors, the source of the problem should be thoroughly investigated and corrected. Many researchers [6, 7] have shown that power suppliers add extra charge for costumers with power factor less than specific limits. Therefore; the scope of this paper is to evaluate the impact of voltage imbalance on the power factor.

II. Determining the instantaneous power factor

Consider a symmetrical three-phase machine supplied from a balanced three-phase power supply in which case the input voltage and current for one phase are given by [8]:

$$v_a = \sqrt{2}V_m \cos(\omega t) \qquad (1)$$

$$i_a = \sqrt{2}I_m \cos(\omega t - \varphi) \qquad (2)$$

The voltage and current phase angles, ωt and $(\omega t - \varphi)$, can be determined simply by converting (1) and (2) into rotating vectors using a proper transformation. In signal processing, an analytical signal is defined as the signal which has no negative frequency components [9]. Any real sinusoid signal may be converted to a positive-frequency complex sinusoid signal simply by generating a phase-quadrature component to serve as the imaginary part. This can be done simply by constructing a filter which has the ability to shift each sinusoidal component by 90^o. This filter has a magnitude of unity at all frequencies and introduces a phase shift of -90^o at each positive frequency and 90^o at each negative frequency. This

transformation is called Hilbert Transform [9]. Consider a real signal which is given by:

$$x(t) = 2\cos(\omega t) = e^{j\omega t} + e^{-j\omega t} \quad (3)$$

The Hilbert Transform $H(t)$ for the signal $x(t)$ can be determined simply by applying the ideal phase shifts to (3) as [16]:

$$H(t) = e^{j(\omega t - 90^o)} + e^{-j(\omega t + 90^o)} \quad (4)$$

$$H(t) = -je^{j\omega t} + je^{-j\omega t} = 2\sin(\omega t) \quad (5)$$

The complex analytic signal $z(t)$which corresponding to the real signal $x(t)$ is:

$$z(t) = x(t) + jH(t) \quad (6)$$

By applying Euler's identity thus, in the sum $x(t) + jH(t)$, the negative-frequency components of $x(t)$ and $jH(t)$ cancel out, leaving only the positive-frequency component. Thus the complex analytic signal $Z(t)$ can be expressed as:

$$z(t) = 2\cos(\omega t) + j2\sin(\omega t) \quad (7)$$

Note that the real analytical signal $x(t)$ has now been transformed to a complex analytical signal $z(t)$ and is in vector form which has the property that all negative frequencies of $x(t)$ have been filtered out [9]. The magnitude C and phase angle θ of the analytical signal $z(t)$ can be determined as:

$$C = \sqrt{[x^2(t) + H^2(t)]} \quad (8)$$

$$\theta = tan^{-1}\left(\frac{H(t)}{x(t)}\right) \quad (9)$$

Converting the input voltage (1) and current (2) into positive-frequency complex signals by applying Hilbert transform will facilitate determining

their phase angles. Similar to (3) the Hilbert transform for v_a and i_a can be determined simply by applying the ideal phase shifts to (1) and (2) hence it can be expressed as [9]:

$$v_H = \sqrt{2}V_m \sin(\omega t) \quad (10)$$

$$i_H = \sqrt{2}I_m \sin(\omega t - \varphi) \quad (11)$$

Therefore, the complex voltage and current analytic signals which corresponding to (1) and (2) can be expressed as [20]:

$$\overrightarrow{v_A} = \sqrt{2}V_m[(\cos(\omega t) + j\sin(\omega t)] \quad (12)$$

$$\overrightarrow{\imath_A} = \sqrt{2}I_m[(\cos(\omega t - \varphi) + j\ \sin(\omega t - \varphi)] \quad (13)$$

Clearly, equations (12) and (13) represent two vectors rotating with an angular velocity ω and shifted from each other by an angle φ as is shown in figure 1. The voltage vector has a magnitude V and a phase angle φ_v while current vector has a magnitude I and a phase angle φ_i. The magnitude and phase angle of the two vectors are:

$$\mathrm{V} = \sqrt{(v_A)^2 + (v_H)^2} \quad (14)$$

$$I = \sqrt{(i_A)^2 + (i_H)^2} \quad (15)$$

$$\varphi_v = \tan^{-1}\left(\frac{v_H}{v_a}\right) \quad (16)$$

$$\varphi_i = \tan^{-1}\left(\frac{i_H}{i_a}\right) \quad (17)$$

where

$\varphi_v = \omega t$ and $\varphi_i = \omega t - \varphi$

It is now possible to verify that the phase shift between the input voltage and current φ is the phase shift between the two rotating vectors. This can be demonstrated mathematically simply by subtracting $\varphi_i$from φ_v as:

$$\varphi = \varphi_v - \varphi_i = \omega t - (\omega t - \varphi) = \varphi \qquad (18)$$

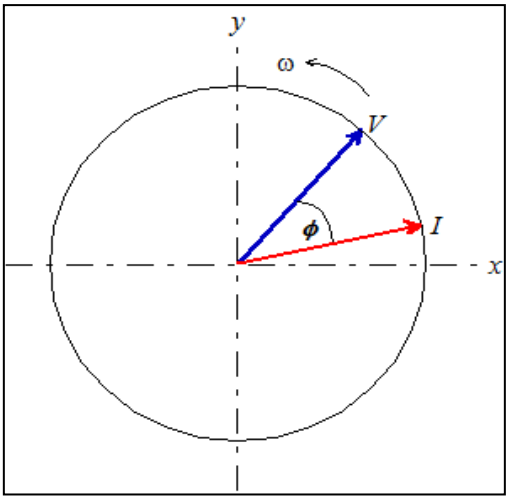

Figure.1: Voltage and current rotating vectors

Taking the cosine of φ gives the instantaneous power factor of the machine.

III. Simulation

Three-phase, 3kW, 415V, 0.8lag, 4-poles, 50Hz cage induction motor model has been developed and validated. The rotor is modelled as multi-coupled circuits, so for a rotor with *n* bars there are *n* rotor loops plus two end ring loops. However, in the absence of an axial flux component, the circumferential currents in the two end rings are zero and do not couple with stator windings hence they were ignored in this model. Therefore the rotor resistance and inductance would be represented by *n* x *n* matrixes. The derivation of induction motor model is beyond the scope of this paper since it can be found in many texts [11and 13]. Therefore only the final equations, which describe the behaviour of a squirrel cage induction motor

under normal and abnormal operating conditions, are presented in this paper.

Modelling of Normal Operating Condition

The stator and rotor voltages under normal operating condition can be expressed in a matrix form as:

$$[V_s] = \left[R_s + \frac{dL_s}{dt}\right][I_s] + [L_s]\frac{d[I_s]}{dt} + [M_{sr}] + \frac{d[I_r]}{dt} + \frac{d[M_{sr}]}{dt} + [I_r] \qquad (19)$$

$$[V_r] = \left[R_r + \frac{dL_r}{dt}\right][I_r] + [M_{sr}]^T\frac{d[I_s]}{dt} + \frac{d[M_{sr}]^T}{dt}[I_s] + [L_r]\frac{d[I_r]}{dt} \qquad (20)$$

Figure 2 shows the flow chart of the mathematical model.

Modelling of Voltage Phase Imbalance Fault

A voltage phase imbalance fault can be introduced in the squirrel cage induction motor model simply by reducing the voltage in one of the three-phases. The stator input voltages are given by [9]:

$$V_s = \sqrt{2}\begin{bmatrix} V_m\cos(\omega t) \\ V_m\cos(\omega t + 120^o) \\ V_m\cos(\omega t + 240^o) \end{bmatrix} \qquad (21)$$

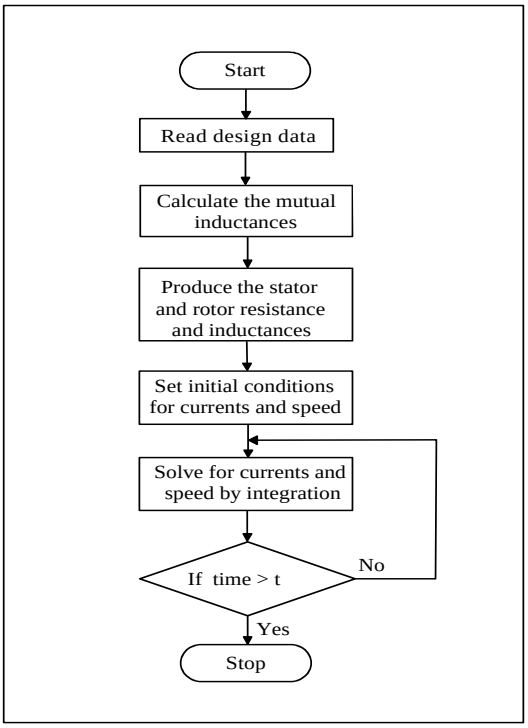

Fig.2: The flow chart of the induction motor model

A voltage imbalance is introduced into Equation (21) by reducing V_m in one row of the matrix by an amount V_d, so the stator voltage which will be used to simulate voltage imbalance is [10]:

$$V_{s(im)} = \sqrt{2}\begin{bmatrix}(V_m - V_d)\cos(\omega t)\\ V_m \cos(\omega t + 120^o)\\ V_m \cos(\omega t + 240^o)\end{bmatrix} \qquad (22)$$

Equation (22) is now substituted back into Equation (19) to give [10, 12]:

$$[V_{s(im)}] = [R_s][I_s] + [L_s]\frac{d[I_s]}{dt} + \frac{d[L_s]}{dt}[I_s] + [M_{sr}]\frac{d[I_r]}{dt} + \frac{d[M_{sr}]}{dt}[I_r] \quad (23)$$

For transient operation, a mechanical model is coupled to the electrical system via the electromagnetic torque which can be determined from a consideration of energy flow through the motor. The mechanical equation of motion depends on the characteristics of the load, which may differ

widely from one user to another. For simplicity, the torque which applied to oppose the electromagnetic torque (produced by the motor) assumed to be an external load and an inertia torque. In this case the mechanical equation of motion is given by [12]:

$$\frac{d\omega}{dt} = \frac{T_{em} - T_{el}}{J} \qquad (24)$$

The electromagnetic torque can be obtained from the magnetic co-energy W_{co} as [12]:

$$T_{em} = \frac{dW_{co}}{d\theta} \qquad (25)$$

In a linear magnetic system the co-energy is equal to the stored magnetic energy [10] so that

$$W_{co} = \frac{1}{2}\begin{bmatrix} I_s \\ I_r \end{bmatrix}^T \begin{bmatrix} L_s & M_{sr} \\ M_{sr} & L_r \end{bmatrix} \begin{bmatrix} I_s \\ I_r \end{bmatrix} \qquad (26)$$

It is obvious from (26) that L_s and L_r contains only constant elements, therefore after some matrix algebra T_{em} can be written as[10]:

$$T_{em} = P[I_s]^T \left(\frac{d[M_{sr}]}{d\theta}\right)[I_r] \qquad (27)$$

IV. Results

During the simulation few important measures were taken for each operating condition. These measures are:

- The simulated motor takes about 1.2 second to reach full speed. To better ensure accurate analysis the investigations presented in this paper except figure 3 were performed beyond this period of time and for two mechanical revolutions.
- For better results the model was run at 50% load under all the operating conditions.

The induction motor model was run under normal operating condition at 50% load. Figure 3 shows the simulated stator current and rotor speed under normal operating condition.

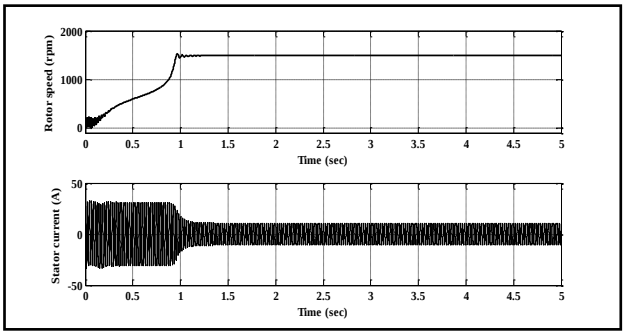

Fig. 3. A-phase stator current and rotor speed for normal operating condition

For further model verification the instantaneous phase shift was determined [6] as explained in section II. Figure 4 shows the simulated instantaneous phase shift and power factor at 50% load under normal operating condition. Clearly the average value of the simulated phase angle φ and power factor ($cos\varphi$) are approximately 37.4^{o} and 0.8 respectively.

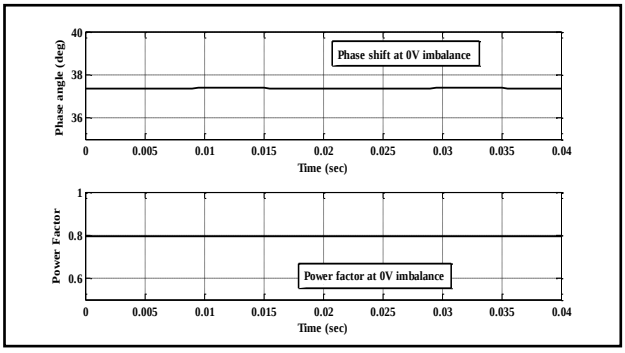

Fig.4. Phase angle and power factor for a normal operating condition

A voltage phase imbalance fault has been introduced in the model as explained above, and then the model was run at 50% load. The instantaneous phase shift was determined under such faulty condition.

Figures 5 and 6 show the simulated instantaneous phase shift and power factor under 10V and 15V voltage imbalance conditions (in time domain).

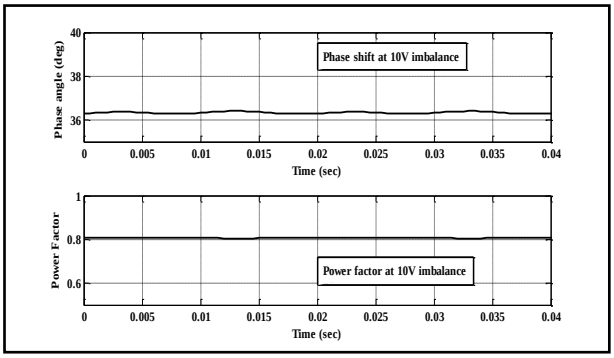

Fig.5. Phase shift and power factor for a 10V imbalance condition

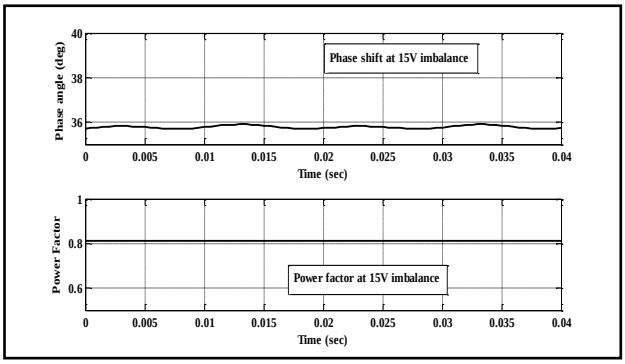

Fig.6. Phase shift and power factor for a 15V imbalance condition

It can be seen from figure 4 that the average value of the instantaneous phase angle is 37.4^{o} while the average value of the power factor found to be 0.8. In comparing figure 4 to figures 5 and 6, one can obviously see the differences in both the phase angle and power factor. The faulty condition cases show that the phase angle decreases to 36.5^{o} while the power factor increases to 0.82 when a 10V imbalance introduced in the model. In the case of 15V imbalance both of the two parameters changes in gradual manner, the phase angle decreases to 35.7^{o} while the power factor increases to 0.83. The obtained results are very much agree with a research carried out by Hahn [13], Lee [14] and Alshandoli [15] which

have been experimentally demonstrated that power factor increases as the voltage imbalance increase.

Although the above results presented in figures 5 and 6 show some change in the system phase angle and power factor, more investigations could be useful in evaluating the effect of voltage imbalance on power factor. Tracking of individual frequency components can be achieved if the power factor is presented in the frequency domain. In addition to this a close correlation with physical system characteristics can be attained. Figures 7 and 8 show the simulated power factor spectra under normal and 10V and 15V imbalance conditions at 50% load. It can be seen that in the normal condition there is no frequency side bands around the supply frequency, while some frequency side bands around the supply frequency are presented under 10V and 15V imbalance cases. It is also clear from the two faulty cases that the amplitude of the side bands increases as the percentage of imbalance increase, so at 10V case the amplitude of the side bands is approximately −60dB while it was −55dB at 15V case.

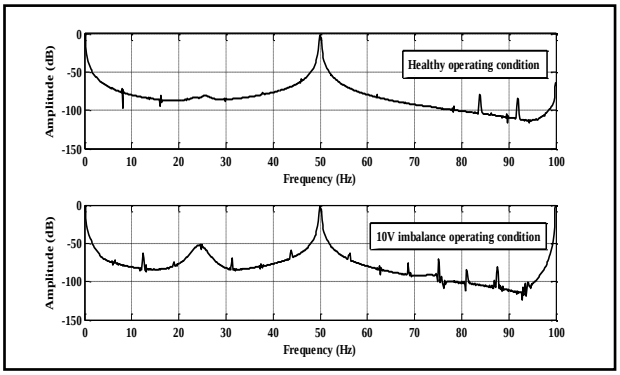

Fig.7. Power factor spectrum for healthy and 10V imbalance

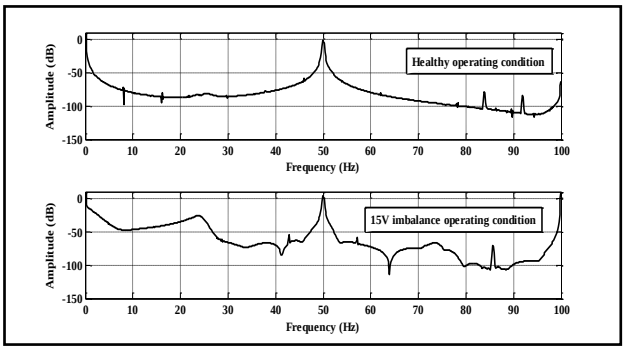

Fig.8. Power factor spectrum for healthy and 15V imbalance

V. Conclusion

The results obtained in this simulation study clearly show that:

- Voltage imbalance has as a very important effect on the power factor of an induction motor.
- The power factor increases as the percentage of voltage imbalance increase.

Based on the above information the following two recommendations are worth to be presented in this paper:

- It is very important for power suppliers to maintain a balanced system in order to prevent extra load on their grid.
- Consumers should inform their power supplier for any changes in voltage in order to avoid an additional charge on their consumption bill.

VI. References

Kang. M, Furong. L, Raj. A, "Quantification of Additional Reinforcement Cost Driven by Voltage Constraint Under Three-Phase Imbalance", IEEE Transactions on Power Systems, Vol. 31, No. 6, pp5126-5134, 2016.

Annette. V. J, "Assessment of Voltage Unbalance", *IEEE Transaction on power delivery*, Vol. 16, No. 4, pp.782-790, October 2001.

Hofmann. P and Pillay. P, “Derating of Induction Motors Operating with a Combination of Unbalanced Voltages and Over- or Undervoltages”, *IEEE Transactions on Energy Conversion*, Vol 17, No. 4 , pp 485-491, Dec 2002.

American National Standard for Electrical Power Systems and Equipment – Voltage Ratings (60 Hertz), ANSI C84.1-1995.

National Electrical Manufacturers Association (NEMA) Publication No. MG 1-1998 Motors and Generators.

Abdelhamed. F. S, "Determining the Instantaneous Power Factor of an Electrical System by the use of Hilbert Transform", *Journal of Engineering Research and Applied Sciences*, Vol.1, No.3, Hoon, Libya, Dec 2016.

Mohammadali. K, Ahmed. F. Z, Maysam. A, *“*Estimating power factor of induction motors using regression technique*”, 17th International Conference on Harmonics and Quality of Power* (ICHQP), pp.502-507, 2016.

Prasanna. K. C, Sabberwal. S. P, Mukharji. A. K, "Power factor measurement and correction techniques", Electrical Power System Research 32, *Indian Institute of Technology*, pp. 141-143, New Delhi, 1995.

Hughes. A, *Electric Motors and Drives-fundamentals, Types and Applications*: Newnes, 2001.

Bracewell. R, *The Hilbert Transform, The Fourier Transform and Its Applications*, 3rd ed: McGraw-Hill, 1999.

Chee-Mun. O, *Dynamic Simulation of Electric Machinery*: Prentice Hall PTR, 1998.

Alshandoli. A.F, Gu. F, and Ball. A.D, "Detection of Induction Motor Faults Using Instantaneous Phase Variation," presented at *Proceedings of ESDA*

2004, 7th Biennial ASME conference Engineering system design and analysis, UK, 2004.

Hahn. M, and Rhr. K, "Dynamic Simulation of an Induction Motor for Healthy Operation and under Fault Conditions", The University of Manchester Socrates Erasmus Exchange Project Report, 2002.

Ching-Yin L, "Effects of Unbalanced Voltage on the Operation Performance of a Three-phase Induction Motor", *IEEE Transactions on Energy Conversion*, Vol. 14, No. 2, pp. 202-208, June 1999.

Alshandoli A.F.S, Ball. A.D, Alzahawi. B.A.T., and Gu. F, "The Use of Instantaneous Phase Variation for Monitoring Three-Phase Squirrel Cage Induction Motors," presented at *Electric Proceedings of the 6th Annual Condition Monitoring and Diagnostic Engineering Management Conference* (COMADEM), 2003.

VII. The Autor

In 1990 Mr Abdelhamed graduated from the Higher Institute of Electrical and Mechanical Engineering Hoon-Libya.

He has worked as a designer Engineer with the General Board of Industry in Libya from 1991-1994, then he was appointed as a lecturer in the Training Centre at the same institution from 1994 to 1995.

In 1997 he has obtained his MSc degree in Electric Power Systems from the University of Manchester Institute of Science and Technology (UMIST) , UK.

Mr Abdelhamed was appointed as a lecturer at the University of Tahadi, Physics department, Libya from 1998-2000.

In September 2001 Mr Abdelhamed commenced his PhD at the University of Manchester, School of Mechanical, Aerospace and Civil Engineering.

In 2005 Mr Abdelhamed has obtained his PhD degree in Mechanical Engineering from The University of Manchester, UK.

Dr Abdelhamed worked as lecturer at the Faculty of Engineering, the 7^{th} of October University, from 2006-2010, and during this period he has appointed as a head of the electrical and electronics department.

In 2008 Dr Abdelhamed has become an assistant professor.

From 2012- 2015 he worked as assistant professor at the faculty of engineering, Zytona university.

Dr Abdelhamed interests in general Machinery Condition monitoring (in particular motor monitoring), Matrix Converter, Polymeric Insulators, Permanent Magnet Machines and advanced Signal Processing, Dr Abdelhamed has published more than 15 technical and professional publications in these fields.

In the meantime he works as the Secretary of the Scientific Affairs at the faculty of engineering, Bani-Walid University.